TRHEE-DIMENSIONAL BOUNDARY LAYER CALCULATION BY A CHARACTERISTIC METHOD

R. Houdeville
O N E R A - C E R T
2 avenue Edouard Belin
31055 TOULOUSE Cedex
FRANCE

Summary

A numerical method for solving the three-dimensional boundary layer equations for bodies of arbitrary shape is presented. In laminar flows, the application domain extends from incompressible to hypersonic flows with the assumption of chemical equilibrium. For turbulent boundary layers, the application domain is limited by the validity of the mixing length model used. In order to respect the hyperbolic nature of the equations reduced to first order partial derivative terms, the momentum equations are discretized along the local streamlines using of the osculator tangent plane at each node of the body fitted coordinate system. With this original approach, it is possible to overcome the use of the generalized coordinates and therefore it is not necessary to impose an extra hypothesis about the regularity of the mesh in which the boundary conditions are given. By doing so, it is possible to limit, and sometimes to suppress, the pre-treatment of the data coming from an inviscid calculation. Although the proposed scheme is only semi-implicit, the method remains numerically very efficient.

1 INTRODUCTION

A great number of three-dimensional boundary layer calculation methods have been developed in the last two decades. Some of them are presented in the synthetic papers of Smith[33], Cousteix[14] and, more recently, Humphreys and Lindhout[17]. Although the amount of work done to solve the Prandtl equations is substantial, some difficulties remain when the crossflow direction changes in the calculation domain. As it has been shown by Wang[35] and Krause[21] this problem comes from the nature of the set of the boundary layer equations which imposes a *CFL* type condition to the discretization scheme (Cebeci et al[9]). To fulfil this condition, at least two solutions may be proposed: i) to choose a simple numerical scheme as, for example, an explicit upwind discretization of the crosswise derivatives ; ii) to use an implicit discretization of the crosswise derivatives at the unknown station.

With the first solution, the advancement of the integration at a given station always goes in the same crosswise direction and the changes of the crossflow, which appear on bodies at incidence, cannot be completely calculated, as shown by Cebeci[9 19 25], unless a change of the discretization scheme across the boundary layer thickness is allowed (Lindhout-Moek[25]). In the second case, the calculation effort is much more important, and therefore reduces the interest in using the Prandtl equations (Patel-Baek[31], Johnston[20]). In practice, a third strategy exists to conciliate the respect of the *CFL* condition with the efficiency of the numerical scheme. Considering only the finite difference methods, Cebeci[9] uses the standard "Keller Box" method everywhere it is possible and the "zig-zag" scheme where the crossflow direction changes. In this latest scheme, the crosswise advection terms are partly written at the calculation station, and partly at the upstream station. To overcome some limitations of this method, Cebeci[9 10 11] proposes the "Characteristic Box Scheme" which takes into account the existence of characteristic directions in the boundary layer equations to limit the streamwise integration step in the region where the crossflow changes sign in the boundary layer thickness. This leads to an extra iteration step at each calculation station.

The numerical scheme which is presented in this paper integrates the Prandtl equations along the local streamlines, which are sub-characteristic lines. By doing so, the integration proceeds always in the same direction whatever the crossflow direction, and the *CFL* condition is fulfilled, providing that the marching step is small enough. As the diffusion terms are expressed at the unknown station, the proposed method belongs to the semi-explicit type.

The main originality of the proposed method comes from the choice of the space in which the equations are integrated. Most methods use generalized coordinates in a body fitted coordinate system. This needs the calculation of the Christoffel coefficients which introduces an extra hypothesis dealing with the regularity of the mesh, while the boundary layer assumptions impose only the regularity of the body surface. To avoid this extra limitation, the discretization of the equations at a given station can be done in the tangent plane to the surface at this point instead of the actual surface. To respect the metric properties of the surface and express the covariant derivatives of the velocity, the tangent plane must be provided with a particular metric. This is simply done by orthogonally projecting the body fitted coordinate system and the velocity field on the tangent plane at the considered points.

2 Boundary layer equations

Body fitted coordinate system

To set up the boundary layer equations, it is convenient to use a body fitted coordinate system (see, for example, Hirschel-Kordulla[16]). Let x^i be the cartesian coordinates of a surface point. This point is known by the two parameters X^1 and X^2. With $\vec{e_i'}$ the cartesian base vector, the vectors defined by

$$\vec{a_\alpha} = \frac{\partial x^i}{\partial X^\alpha} \vec{e_i'} \qquad \alpha = 1,2 \qquad i = 1,2,3 \qquad (1)$$

are tangent to the body fitted coordinate system.

The surface base reference frame is obtained by adding the unity vector $\vec{a_3}$ perpendicular to $\vec{a_1}$ and $\vec{a_2}$. The reference frame $(\vec{e_1}, \vec{e_2}, \vec{e_3})$ in the vicinity of the surface is built as shown in figure 1. Introducing the thin layer assumption, the metric elements $g_{ij} = \vec{e_i}.\vec{e_j}$ become independent of the X^3 coordinate.

The boundary layer equations are obtained by applying the Prandtl hypothesis to the Navier-Stokes equations written in the curvilinear coordinates $(X^i, i = 1,2,3)$.

For an incompressible laminar flow, the boundary layer equations read :

$$\nabla_i U^i = 0 \qquad i = 1,2,3 \qquad (2a)$$

$$\rho U^i \nabla_i U^\alpha = -\nabla_\alpha P + \frac{\partial}{\partial X^3}\left(\mu \frac{\partial U^\alpha}{\partial X^3}\right) \qquad \alpha = 1,2 \qquad (2b)$$

The covariant derivatives of the velocity are expressed using the Christoffel coefficients:

$$\nabla_i U^\alpha = \frac{\partial U^\alpha}{\partial X^i} + \Gamma^\alpha_{ij} U^j \qquad (3)$$

In the equations 2a and 2b, the pressure field is known. It is, for example, the wall pressure given by an inviscid calculation. The boundary conditions are the no-slip condition at the wall and the velocity components U_e^α, (with $\alpha = 1,2$) at the outer edge of the boundary layer. The latter can be obtained from the pressure field by integrating the Euler equations at the wall.

Nature of the set of equations

From the theory of quasi linear differential equations, the boundary layer equations 2a and 2b are parabolic because of the diffusion terms. It has been shown by Wang[35] and Krause[21] that the particular influence of the advection terms could be studied from the characteristic surfaces of the subset of equations made of the first order derivatives. They have shown that the surfaces made of the straight lines perpendicular to the wall and the stream surfaces are sub-characteristic surfaces. This means that the influence domain of a particular station is limited by the two surfaces, formed of perpendicular lines to the wall, which are tangent to the two most deviated streamlines.

3 Numerical method

A great number of calculation methods have been developed to integrate the boundary layer equations in direct mode, *i.e.* with a prescribed external velocity field. Some reviews of these methods can be found in Smith[33], Cousteix[14] and Humphreys-Lindhout[17]. Most of these methods are space-marching, with an upstream discretization of the advection terms.

Lindhout-Boer[24] made a semi-implicit method in which the crosswise derivatives along X^2 are explicitly discretized in the upstream direction, the other derivatives being written implicitly. This allows a change of the crossflow direction to be taken into account very simply. The calculation step in the streamwise direction is limited by a *CFL* condition. To avoid this constraint, it is necessary to express implicitly the X^2-derivatives. This can be done simply if the dependence domains remain in a given side of the mesh lines X^1 in the whole calculation domain (fig. 2a). For such flows, for example flows over infinite swept wings, the calculation advances everywhere in the same direction along the X^1 lines. Jelliti[19] and Barberis[6] used this technique. For more complex boundary layer flows, such methods do not allow accessibility to the domains for which the crossflow does not remain in the marching direction along the X^1 lines.

Lindhout *et al.*[25] have developed a technique in which the choice of the numerical scheme for the crosswise derivatives in the X^2 direction and the marching sense along these lines depend on the most deviated streamlines throughout the boundary layer at the calculation station. This allows a certain optimization of the calculation effort by choosing in each region the most suitable discretization.

Other methods have been considered. An efficient scheme of the "predictor-corrector" type is used by Matsuno[27]. Wang[36] has proposed a"zig-zag" scheme in order to take into account the dependence domains for the discretization of the velocity along the X^2 direction. These terms are written partly at the known upstream station and partly at the unknown calculation station, on both sides of the corresponding X^1 line. The stability of this scheme is discussed by Krause[21]. A similar scheme has been used also by Iyer *et al.*[18] and Cebeci[9]. This author prefers a modified version of the "Keller box scheme", called the "characteristic box scheme" which takes into account the dependence domains by using the direction of the local streamline in the discretization formulation. This leads to an extra iteration step at each station and a limitation of the marching step in the X^1 direction[11].

Fully implicit techniques in which the X^2-derivatives are written in the unknown plane $X^1 = Cste$ (fig. 2a) can be considered. Patel-Baek[31] and Tassa *et al.*[34] use the alternated direction procedure to solve the equations in a whole plane $X^1 = Cste$. Johnston[20] prefers to sweep only in the X^2 direction, which leads to iterative inversion of tridiagonal matrices; the unknown quantities being taken at the previous iteration.

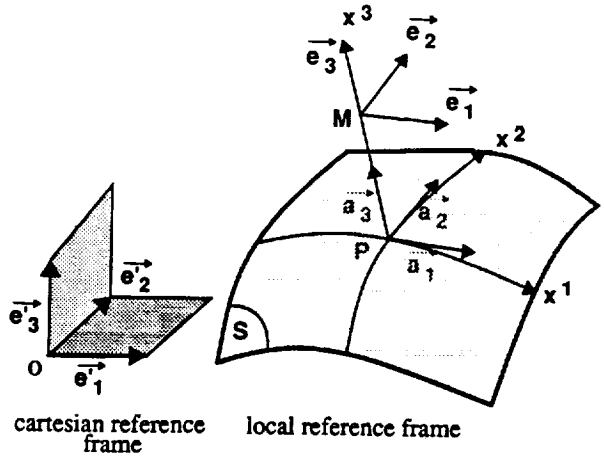

Figure 1 : Body fitted coordinate system and wall reference frame.

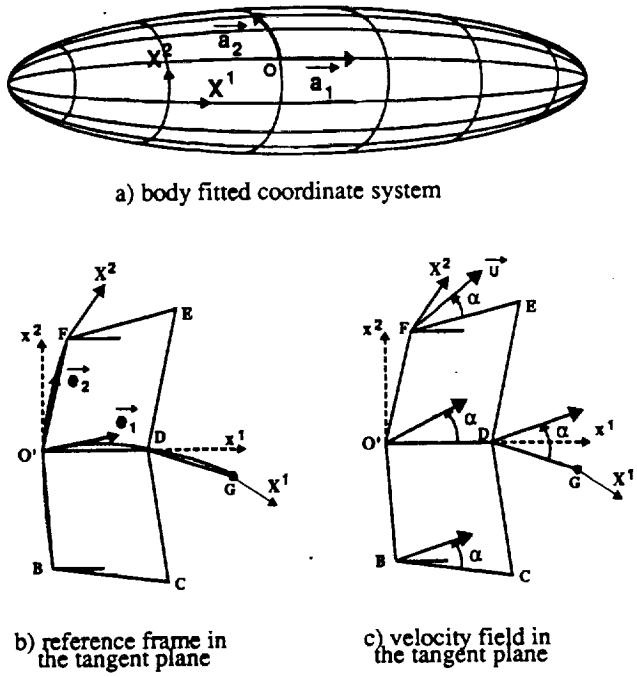

Figure 2 : Building of the calculation mesh and velocity field in the tangent osculator plane.

Equations along the local streamlines

In order to respect the physical dependence domains at each point of the boundary layer while keeping a single marching direction along the X^2-lines, the momentum and energy equations will be discretized along the local streamlines. This also allows the use of a unique scheme in the whole calculation domain.

As is usually done in boundary layer calculations, a reference length $L(X^1, X^2)$ is introduced to adapt the grid perpendicular to the wall to the boundary layer thickness. With the normal coordinate $\eta = X^3/L(X^1, X^2)$, the boundary layer equations along the local streamlines read

$$\nabla_{,}\rho U^i + \frac{\partial \rho \overline{U^3}}{L\partial\eta} = -\frac{\rho}{L}U^i\frac{\partial L}{\partial X^i} \qquad i = 1,2 \text{ (4a)}$$

$$\rho\left|\overrightarrow{U}\right|\frac{\nabla U^\alpha}{\mathrm{d}s(\eta)} + \rho\overline{U^3}\frac{\partial U^\alpha}{L\partial\eta} = \rho_e\left|\overrightarrow{U_e}\right|\frac{\nabla U_e^\alpha}{\mathrm{d}s(\delta)} + \frac{\partial}{L^2\partial\eta}\left(\mu_{eff}\frac{\partial U^\alpha}{\partial\eta}\right) \qquad \alpha = 1,2 \text{ (4b)}$$

with

$$\overline{U^3} = U^3 - \eta U^i\frac{\partial L}{\partial X^i} \qquad i = 1,2 \qquad (5)$$

$\mathrm{d}X^1$ being the step size in the main marching direction, $\mathrm{d}s(\eta)$ is calculated using the metric coefficients

$$\mathrm{d}s(\eta) = \left(g_{ij}\,\mathrm{d}X^i_{sl}\mathrm{d}X^j_{sl}\right)^{1/2} \qquad i,j = 1,2 \qquad (6)$$

where $\mathrm{d}X^2_{sl}$ is a function of η obtained from the definition of the local streamline parallel to the wall

$$\frac{\mathrm{d}X^1_{sl}}{U^1} = \frac{\mathrm{d}X^2_{sl}}{U^2} \qquad (7)$$

∇U^i is the total variation of the velocity component U^i along the streamline

$$\nabla U^\alpha = \left(\frac{\partial U^\alpha}{\partial X^i} + \Gamma^\alpha_{ij}U^j\right)\mathrm{d}X^i_{sl} \qquad i,\alpha = 1,2 \qquad (8)$$

Osculator tangent plane

The use of generalized coordinates introduces an extra hypothesis concerning the regularity of the body fitted coordinate system which must be regular enough to allow the calculation of the Christoffel coefficients. Moreover, as the calculation method is of semi-implicit type, the respect of the *CFL* condition leads to the use of a subgrid for the integration in the X^1-direction. The calculations can be done more rapidly if the equations are written in a cartesian coordinate system. Due to the local character of the boundary layer problem, confined to the vicinity of the body surface, it is not the global cartesian frame used to define the surface which will be considered, but a local cartesian frame linked to a mesh of the body fitted coordinate system in which the boundary conditions are given.

To build the osculator tangent plane, it will be assumed that the Christoffel symbols are defined, in order to show that the new approach is identical to the classic one, but this assumption is not necessary.

Let O be the node (X^1_i, X^2_j) of the mesh in which the boundary conditions are given. The local reference frame at this point is $\overrightarrow{e_i}$, $i = 1,2,3$. To integrate the boundary layer equations to the next station (X^1_{i+1}, X^2_j), it is necessary to represent in a cartesian space the neighbouring nodes with respect to point O as well as the velocity vectors (fig 3). To this end, at the point O of the surface (S) is associated a

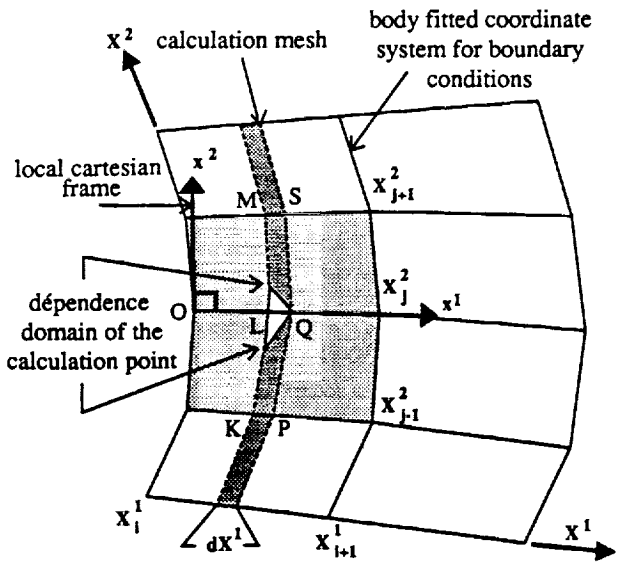

Figure 3 : Sub-calculation mesh with respect to the representation of the body fitted coordinate system in the tangent plane.

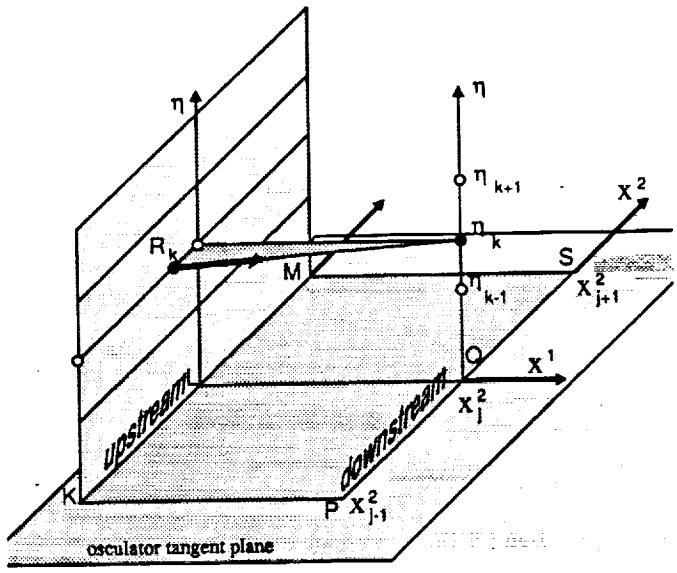

Figure 4 : Discretization of the momentum and energy equations.

point O' of an euclidian space (E). The reference frame $(\overrightarrow{e_i'}, i = 1,2)$ at this point is such that

$$\overrightarrow{e_i'}\Big)_{O'} = \overrightarrow{e_i}\Big)_O \qquad (9)$$

This leads to the equality for the metric elements

$$g_{ij})_{O'} = g_{ij})_O \qquad (10)$$

It can be noted that if the points O and O' are identical, the euclidian space (E) which has been built is simply the tangent plane to the surface at O. In order to give to (E) the metric properties that represent the vicinity of point O of (S), we impose

$$\Gamma^k_{ij}\Big)_{O'} = \Gamma^k_{ij}\Big)_O \qquad (11)$$

This allows to represent the body fitted coordinate system in the vicinity of point O by a curvilinear coordinate system in the tangent plane while respecting the distances to the second order (fig. 2-b). For this reason, the tangent plane is called osculator plane. With the condition (11), the image P' in (E) of a point P in (S) near the point O is given by

$$\overrightarrow{O'P'} = \left(\overrightarrow{e_i}\right)_O \left[dx^i + \frac{1}{2}\left(\Gamma^i_{jk}\right)_O dx^j dx^k\right] \qquad (12)$$

After the construction of the mesh in the neighbourhood of O in the tangent plane, the representation of the velocity field is simply done: the velocity vectors are known, for example, by their modulus and directions with respect to the lines X^1 on the surface. The directions with respect to the curvilinear mesh in the tangent plane are assumed to be the same (fig. 2-c). Knowing the geometry of the mesh and the velocity at the nodes, the calculation of the covariant derivatives of the velocity is straightforward. With the representation which has been adopted, the precision of this calculation is of first order.

The covariant derivative of a vector is an intrinsic quantity which does not depend on the reference mesh. This quantity exists even if discontinuities of the slope of the coordinate lines are present. In this case, the Christoffel coefficients are not defined and the velocity components are discontinuous. Such a configuration can be dealt with if the osculator tangent plane is built without using the Christoffel coefficients. It can be shown that the construction which has been described is equivalent to the orthogonal projection of the body fitted coordinate system, and the velocity field, in the tangent plane at a given point. This transformation respects the lengths and the angles to the second order, which allows to express the covariant derivatives to the first order.

Basic equation

It has been shown that the integration of the boundary layer equations could be done in the tangent plane instead of using the generalized coordinates. For this reason, the equations can be written in cartesian coordinates. For a compressible turbulent boundary layer, equations (2a), (4a) and the energy equation become

$$\frac{\partial \rho u^i}{L\partial x^i} + \frac{\partial \rho \overline{u^3}}{L\partial \eta} = -\frac{\rho u^i}{L}\frac{\partial L}{\partial X^i} \qquad i = 1,2 \qquad (13a)$$

$$\rho\left|\overrightarrow{u}\right|\frac{du^\alpha}{ds(\eta)} + \rho\overline{u^3}\frac{\partial u^\alpha}{L\partial\eta} = \rho_e\left|\overrightarrow{u_e}\right|\frac{du_e^\alpha}{ds(\delta)} + \frac{\partial}{L^2\partial\eta}\left(\mu_{eff}\frac{\partial u^\alpha}{\partial\eta}\right) \qquad \alpha = 1,2 \qquad (13b)$$

$$\rho\left|\overrightarrow{u}\right|\frac{\mathrm{d}h_i}{\mathrm{d}s(\eta)}+\rho\overline{u^3}\frac{\partial h_i}{L\partial\eta} = \frac{\partial}{L^2\partial\eta}\left[\frac{\lambda_{eff}}{C_p}\frac{\partial h_i}{\partial\eta}+\left(\mu_{eff}-\frac{\lambda_{eff}}{C_p}\right)\frac{\partial}{2L\partial\eta}\left((u^1)^2+(u^2)^2\right)\right] \quad (13c)$$

with

$$\overline{u^3}=u^3-\eta\left(u^1\frac{\partial L}{\partial x^1}+u^2\frac{\partial L}{\partial x^2}\right) \quad (14)$$

and the equation of the streamline parallel to the wall

$$\frac{\mathrm{d}x^1}{u^1}=\frac{\mathrm{d}x^2}{u^2} \quad (15)$$

$\mathrm{d}x^1$ is given by the marching step along the x^1-lines, roughly in the general direction of the flow. $\mathrm{d}u^\alpha$ is the variation of the u^α-component of the velocity over the distance ds along a streamline. The energy equation (13c) is written for the total enthalpy h_i

$$h_i = C_pT+\frac{\left|\overrightarrow{U}\right|^2}{2} \quad (16a)$$

and the effective viscosity coefficient is expressed as follows

$$\mu_{eff} = \mu+\gamma\mu_t \quad (17a)$$

where μ is the dynamic viscosity coefficient given by the law of Sutherland, μ_t the eddy viscosity coefficient and γ the intermittency function which is equal to 0 for laminar flow and 1 in turbulent boundary layer. In the transition region, γ depends on the thickening of the boundary layer represented by the ratio of the momentum thickness to the momentum thickness at the beginning of the transition region, θ/θ_T[4].

Since the first objective of this study is the validation of the numerical technique, including the discretization scheme and the use of the osculator tangent plane, a simple turbulence model is used. The model is a direct extension of the mixing length formulation commonly used in two-dimensional flows[12], with the damping function proposed by Cebeci [8]

$$\tau_{x^1} = \mu\frac{\partial u^1}{\partial x^3}-\rho\overline{u'^1u'^3}=(\mu+\mu_t)\frac{\partial u^1}{\partial x^3} \quad (18a)$$

$$\tau_{x^2} = \mu\frac{\partial u^2}{\partial x^3}-\rho\overline{u'^2u'^3}=(\mu+\mu_t)\frac{\partial u^2}{\partial x^3} \quad (18b)$$

$$\mu_t = \rho l^2F^2\sqrt{\left(\frac{\partial u^1}{\partial x^3}\right)^2+\left(\frac{\partial u^2}{\partial x^3}\right)^2} \quad (18c)$$

$$\frac{l}{\delta} = 0,085\tanh\left(\frac{0,41}{0,085}\frac{x^3}{\delta}\right) \quad (18d)$$

with

$$F = 1-\exp\left(-\frac{y^+}{A}\right) \qquad y^+=\frac{yu_\tau}{\nu} \quad (19a)$$

$$A = \frac{26}{N}\frac{\nu}{u_\tau}\sqrt{\frac{\rho}{\rho_w}} \qquad u_\tau=\sqrt{\tau_w/\rho} \quad (19b)$$

$$N = \sqrt{1-11,8\frac{\mu_w}{\mu_e}\left(\frac{\rho_e}{\rho_w}\right)\left(\frac{\nu_e u_e}{u_\tau^3}\frac{\mathrm{d}u_e}{\mathrm{d}s_e}\right)} \quad (19c)$$

In these relations, only applicable in a cartesian reference frame, u_e is the modulus of the external velocity and the friction velocity .

Laminar-turbulent transition

Longitudinal instability mode

Two criteria are used to predict the onset of transition. Both are based on stability calculations for the self-similar Falkner-Skan velocity profiles and on the relation proposed by Mack[26] to link the total amplification coefficient n of the most unstable instability waves, at the point of transition, to the turbulence level of the external flow

$$n_T=-2.4\ln T_u-8.43 \quad (20)$$

In a first criterion proposed by Arnal *et al.*[1], the velocity profile is characterized by the mean value of the Pohlhausen parameter $\overline{\Lambda_2}$, and n is represented as a function of $(R_{\theta_{11}}-R_{\theta_{11cr}})$ and $\overline{\Lambda_2}$

$$R_{\theta_{11}}-R_{\theta_{11cr}} = -206\exp\left(25.7\,\overline{\Lambda_{2T}}\right)\left[\ln\left(16.8\,T_u\right)-2.77\,\overline{\Lambda_{2T}}\right] \quad (21a)$$

$$\overline{\Lambda_2} = \frac{1}{x-x_{cr}}\int_{x_{cr}}^{x}\frac{\theta_{11}^2}{\nu}\frac{\mathrm{d}u_e}{\mathrm{d}x}\,\mathrm{d}x \quad (21b)$$

To determine the critical value of the momentum thickness θ_{11cr} corresponding to the point x_{cr} , the calculated value of θ_{11} is compared to the corresponding value of θ_{11cr_s} given by the stability diagrams and represented by the correlation

$$\theta_{11cr_s}=\exp\left(\frac{52}{H_i}-14.8\right) \qquad H_i=\frac{\delta_1 i}{\theta_{11i}} \quad (22)$$

As soon as $R_{\theta_{11}}$ becomes equal to $R_{\theta_{11cr_s}}$, the instability waves become amplified and x_{cr} is reached.

The second longitudinal criterion, proposed by Arnal[4], is a parametric type method. For a given velocity profile, characterized by the shape parameter H_i, the local amplification coefficient σ, corresponding to the frequency F, is represented as a function of R_{δ_1} in the form of two half-parabols. This allows a simplified representation of the stability diagrams with a minimum number of parameters. Knowing the evolution of the shape parameter H along an external streamline, the total amplification coefficient is calculated and equation (20) is used to determine the onset of transition.

Streamwise instability mode

To predict this mode of transition particular to three-dimensional flows, two criteria can be used. The first one is an extension made by Coustols[15] of a criterion originally proposed by Beasley[7]. The transition occurs when the Reynolds number based on the streamwise displacement thickness δ_2 becomes larger than a critical value which is a function of the

longitudinal incompressible shape parameter. More precisely, this criterion reads

$$R_{\delta_2 T} = 95.5 \arctan\left(\frac{0.106}{(H_i - 2.3)^{2.052}}\right) \qquad 2.3 < H_i < 2.7 \qquad (23a)$$

$$R_{\delta_2 T} = 150 \qquad H_i < 2.3 \qquad (23b)$$

With this criterion, the influence of the turbulence level of the external flow is not taken into account.

The second criterion, also developed by Coustols and Arnal[4 3] requires a more important numerical effort and cannot be detailed here. At each calculation station, the most unstable direction ϵ of the velocity profiles in the vicinity of the crossflow direction must be determined. The transition occurs when the Reynolds number defined with the displacement thickness in the ϵ direction becomes larger than a given value which is a function of the turbulence level of the external flow. The number and location of the inflection points of the velocity profile in the ϵ direction are also taken into account in order to represent the results of stability calculations for three-dimensional boundary layers.

Numerical scheme

The momentum and energy equations (13b) (13c) are discretized in the tangent plane according to the scheme presented in figure 4. At the unknown station Q, the diffusion terms are written at 3 points and the advection term is taken between the points R_k and η_k. R_k is the origin at the upstream station of the streamline going through the point η_k. At this stage, all the quantities are known. R_k is calculated according equation (15) assuming a linear variation of the velocity components at the upstream stations. This discretization scheme leads, after linearization, to three tridiagonal matrices which can be inverted independently to give the two velocity components u^1 and u^2 and the total enthalpy h_t. The scheme is stable whatever the location of points R_k may be. In practice, the marching step along X^1 is limited in order that R_k remains between the two adjacent stations K and M of the calculation point (fig.4). This constraint is identical to the *CFL* condition of a semi-explicit scheme.

To complete the integration, the normal velocity component u^3 is calculated using the continuity equation (13a).

The x^1-derivatives are taken between the points L and Q and the x^2-derivatives are deduced from the relation

$$\left(\rho u^2\right)_M - \left(\rho u^2\right)_K = \left(\frac{\partial \rho u^1}{\partial x^1}\right)_L (x_M - x_K) + \left(\frac{\partial \rho u^2}{\partial x^2}\right)_L (z_M - z_K) \qquad (24a)$$

with x^1 and x^2 the cartesian coordinates in the tangent plane defined in figure 3.

At each station X^1, the boundary layer parameters are calculated for all the points in the X^2 direction. This is always done in the direction of the increasing values of X^2, whatever the crossflow direction may be, because the calculation at a particular station is independent of the neighbouring points. The process is repeated in the subgrid calculation in the X^1 direction up to the station X^1_{i+1} of the body fitted coordinate system in which the boundary conditions are given. At this point, the change of direction α of the coordinate system must be taken into account. Since it is imposed that the calculation subgrid coincides with the station X^1_{i+1}, α does not have to be necessarily small. This means that slope discontinuities of the reference mesh can be correctly treated. A new osculator tangent plane is calculated at each node X^2_j of the station X^1_{i+1} and the calculation process continues.

4 APPLICATION TO A PROLATE SPHEROID

To illustrate some capabilities of the method to predict complex three-dimensional boundary layers, we will consider the prolate spheroid with an aspect ratio equal to 6 at a 10° incidence. A number of experimental studies have been devoted to this case, in particular at the DLR [28 29 30]. At the chosen incidence, the experimental pressure field remains close to the analytical inviscid pressure field. Moreover, the stagnation point is sufficiently close to the nose of the body to use the simple body fitted coordinate system made of ellipses passing through the two poles and circles included in planes perpendicular to the symmetry axis of the body.

In figure 5-c, the light lines show the inviscid streamlines at the wall and the thickest lines represent the friction lines for a fully laminar boundary layer. The friction lines converge to form the separatrice line[23 32]. Along it, a strong thickening of the boundary layer occurs, leading to the abandon of the corresponding calculation line after $X/L = 0.8$. Figure 5-a shows the wall friction lines obtained by taking into account the transition phenomenon. With $R_L = 1.6\ 10^6$ and a turbulence level equal to $1.5\ 10^{-3}$, the boundary layer remains laminar in the windward side up to the separation line, and turbulent in the leeward side. In the latter side, the accumulation of the friction lines for $X/L > 0.7$ can be interpreted as a secondary separation. In figure 5-b are plotted the friction lines calculated by Meier *et al.*[29 30] from measurements of the skin friction. At a 10° incidence, the influence of the flow separation on the pressure field remains small which explains the good agreement concerning the location of the separation line in figures 5-b and 5-a. The comparison of figures 5-a and 5-c shows the great influence of the transition phenomenon.

The same results are presented in figure 6 at a higher Reynolds number of $7.2\ 10^6$. The transition to turbulence occurs sooner, which leads to the displacement of the separation line towards the leeward region and suppresses the secondary separation.

In figure 7 are plotted the longitudinal and streamwise displacement thicknesses δ_1 and δ_2 as well as the shape parameter. They are compared to experimental results obtained by Meier et al at $X/L = 0.64$ and 0.71. The development of separation is characterized by a thickening of δ_1 and

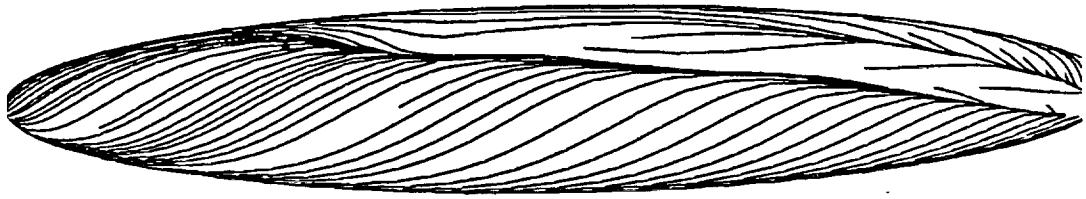

a) with transition criteria. $R_e = 1,6\ 10^6 \quad T_u = 1.5\ 10^{-3}$

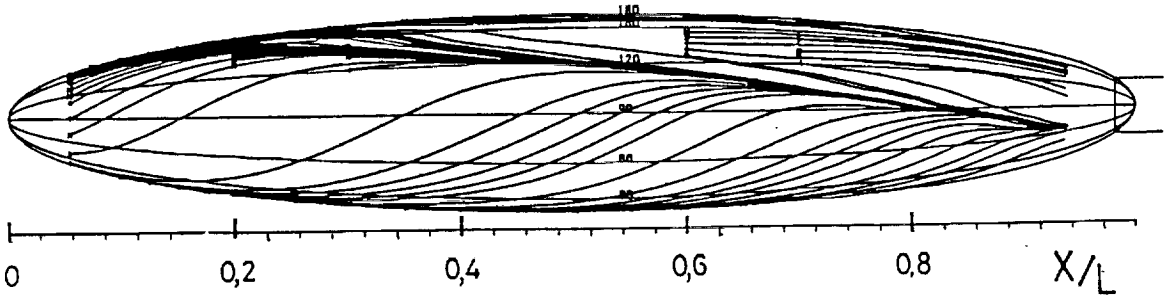

b) experimental results from DLR^{30}

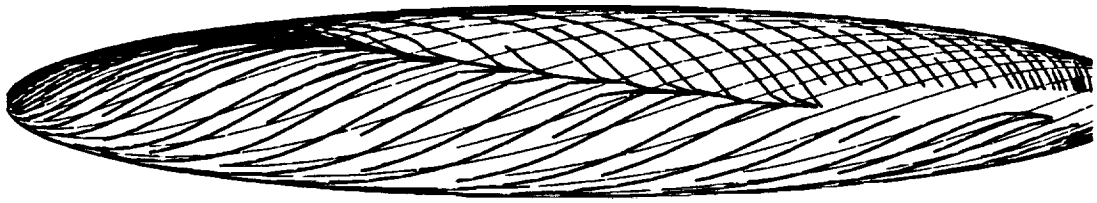

c) laminar calculation

Figure 5 : Ellipsoide at 10° incidence.

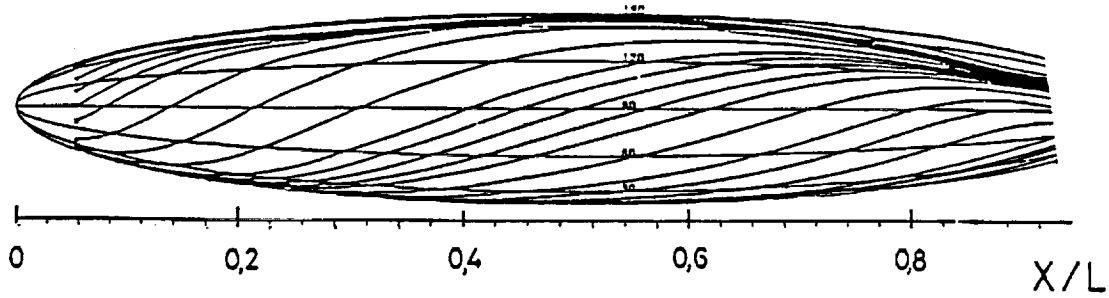

a) experimental results from DLR^{30}

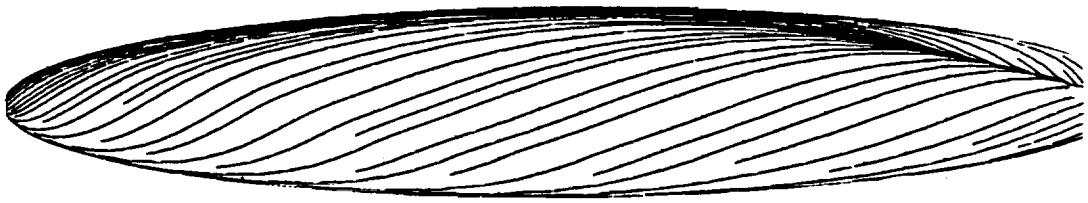

b) wall friction lines.
$R_e = 7,2\ 10^6 \quad T_u = 1.5\ 10^{-3}$.

Figure 6 : Ellipsoide at 10° incidence.

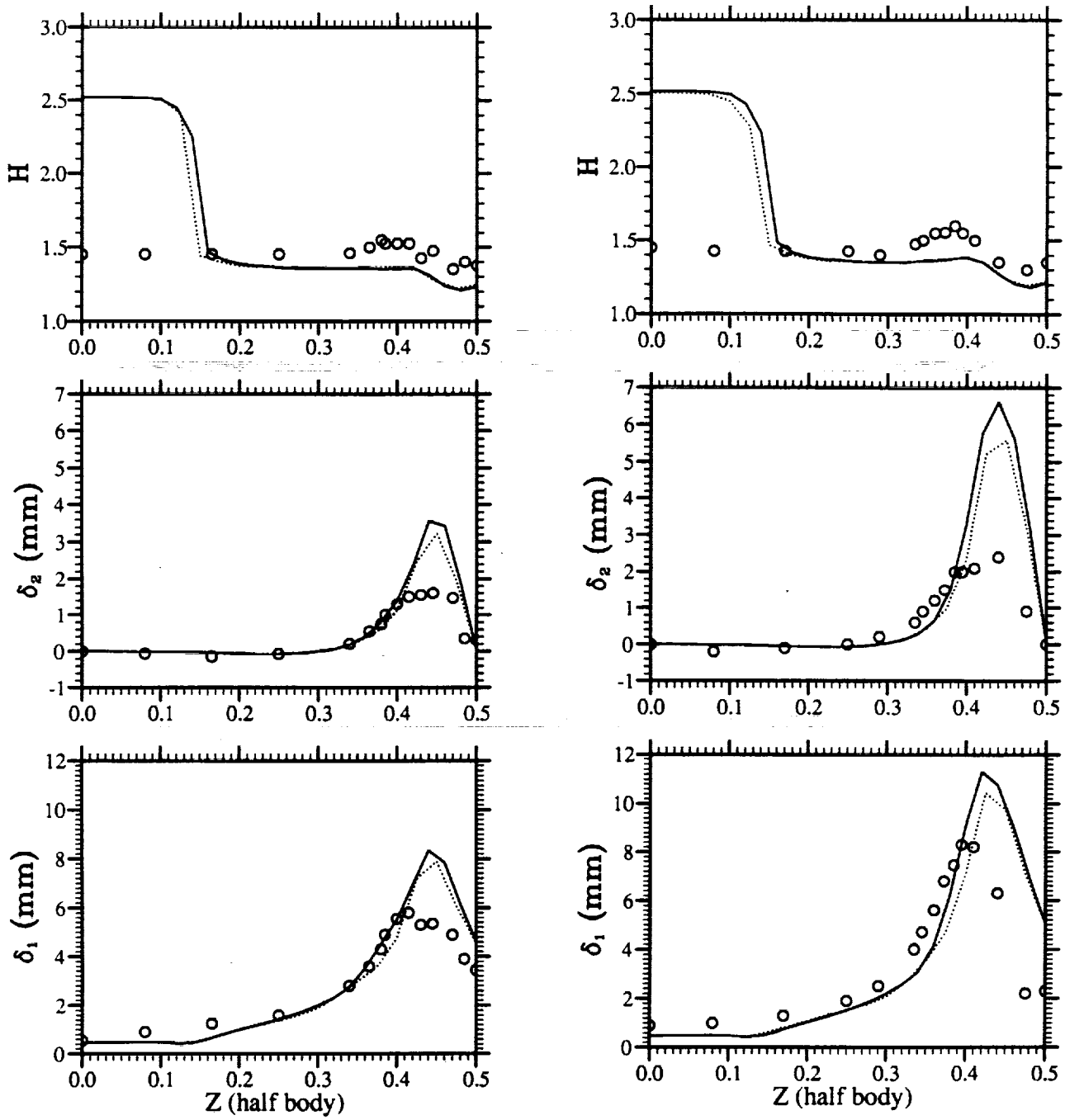

Figure 7 : Ellipsoide at 10° incidence.

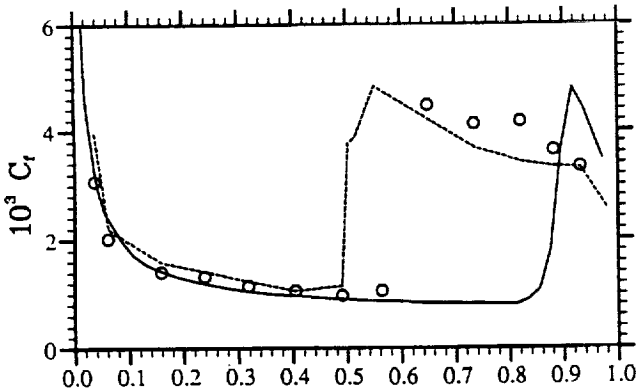

a) windward symmetry line

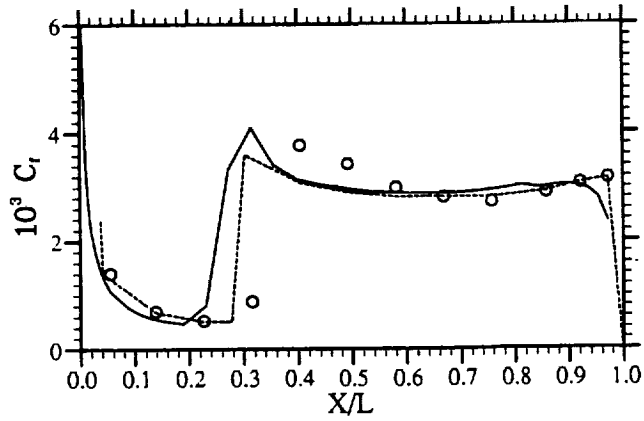

b) leeside smmetry line

present method
Barberis[6] (fixed transition)
o experiment[22]

$R_e = 7,2\ 10^6 \quad T_u = 1.5\ 10^{-3}$

Figure 8 : Ellipsoide at 10° incidence.

δ_2, particularly important at $X/L = 0.71$. The evolution of the longitudinal shape parameter H is mainly sensitive to the nature of the boundary layer. To perform the calculation with the present method, the analytical inviscid flow field has been used as well as the experimental pressure field. The influence on the results remains small. The most critical point concerns the prediction of the transition. The external turbulence level is equal to $1.5\ 10^{-3}$, as in the experiments. With the present calculation methods all the transition criteria have been set active and the first one to predict transition is retained. As it can be seen in the evolution of H in figure 7, the location of the onset of the transition near the windward plane of symmetry is not correctly predicted. This is difficult to explain because the transition occurs along this line by amplification of the longitudinal instability waves which are calculated by the second criterion[5]. Maybe the use of the linear instability theory along a symmetry line with a divergent flow from this line must be questioned. Figure 7, showing the skin friction evolution along the windward and leeward lines in the symmetry plane, indicates that the calculated transition point is located at $X/L = 0.85$ with a turbulence level equal to $1.5\ 10^{-3}$. This turbulence level gives the correct location of the transition line in the lee side region of the body. Its experimental value is estimated between 1 and $2\ 10^{-3}$. By taking the largest value of turbulence level, the transition occurs at $X/L = 0.73$ on the windward symmetry line, instead of 0.65 experimentally, but it reaches 0.17 on the upper symmetry line.

Calculation time

In the present method, the marching step in the X^1 direction is limited by the most deviated streamline at a given section. This step is also limited with respect to the boundary layer thickness δ. For the prolate spheroid, the marching step was limited to be in the range $0.6\delta_{min}$ and $2\delta_{max}$, the minimum and maximum values being taken in every section X^1. With this condition, roughly 1000 calculation steps are needed in the X^1 direction. With 26 lines in the azimutal direction (for a half-body), this corresponds on a CRAY XMP to 10 s for a fully laminar boundary layer and 30 s with all the transition criteria.

5 CONCLUSION

The three-dimensional boundary layer calculation method which has been presented is of semi-implicit type. The advection terms are discretized along the local streamlines. The dependence domains are thereby satisfied with a simple numerical scheme. The counterpart is a limitation on the size of the marching integration step. Despite this limitation, the efficiency of the method remains good due to the reduced amount of calculation at each step. This is partly a consequence of the use of local cartesian coordinates. The discretization of the equations in the osculator tangent plane allows the existence of slope discontinuities in the body fitted coordinate system in which the boundary conditions are given. It also often reduces or suppresses the pre-treatment phase of the data for a calculation.

Although the application cases which have been presented only deal with the prolate spheroid at incidence in incompressible flow, the application range of the code is very large. It extends from subsonic to hypersonic flows.

For turbulent boundary layers, the mixing length model which is used up to now is restrictive. The introduction of transport equation model is being done. It has also been tested that the present method can run in the inverse mode with only minor modifications.

Références

[1] **D. Arnal** : *Laminar-turbulent transition problems in supersonic and hypersonic flows.* AGARD/FDP/VKI Special Course "Aerothermodynamics of Hypersonic Vehicles", Rhode-Saint-Genèse, 30 may-3 june 1988

[2] **D. Arnal** : *Transition prediction in transonic flow* IUTAM Symposium Transsonicum III DFVLR-AVA Göttingen 1988

[3] **D. Arnal, E. Coustols** :*Application de critères bi- et tridimensionnels au calcul de la transition et de la couche limite d'ailes en flèche* Symposium AGARD "Improvement of aerodynamic performance through boundary layer control and high lift systems" Bruxelles may 1984

[4] **D. Arnal, E. Coustols, J.C. Juillen** : *Transition sur une aile en flèche infinie.* La Recherche Aérospatiale 1984-4 (1984)

[5] **D. Arnal, M. Habiballah, E. Coustols** : Laminar instability theory and transition criteria in two and three-dimensional flows. La Recherche Aérospatiale 1984-2 (1984) p. 45-63

[6] **D. Barberis** : *Calcul de la couche limite tridimensionnelle en modes direct ou inverse sur des obstacles quelconques.* La Recherche Aérospatiale, 1986-3 p.169-195

[7] **J.A. Beasley** :*Calculation of the laminar boundary layer and the prediction of the transition on a sheared wing.* ARC R&M 3787 1973

[8] **T. Cebeci, A.M.O Smith** : *Analysis of turbulent boundary layers.* Academic Press 1974

[9] **T. Cebeci, A. K. Khattab, K. Stewartson** : *Three-dimensional laminar boundary layers and the ok of accessibility.* J. Fluid Mech. (1981), Vol.107, pp. 57-87

[10] **T. Cebeci** : *Problems and opportunities with three-dimensional boundary layers.* AGARD May 1984

[11] **T. Cebeci** : *An approach to practical aerodynamic configurations.* V.K.I Lecture Series, 14-18 april 1986

[12] **J. Cousteix, C. Quemard, R. Michel** : *Application d'un schéma amélioré de longueur de mélange à l'étude des couches limites turbulentes tridimensionnelles.* AGARD CP N°93 on "Turbulent Shear Flows" (1971)

[13] **J. Cousteix** : *Analyse théorique et moyens de prévision de la couche limite turbulente tridimensionnelle.* T.P. ONERA 157, 1974

[14] **J. Cousteix** : *Three-dimensional boundary layers. Introduction to calculation methods* AGARD REPORT N°741

[15] **E. Coustols** : *Stabilité et transition en écoulement tridimensionnel : cas des ailes en flèche.* Thèse de Docteur-Ingénieur ENSAE (Juin 1983)

[16] **E. H. Hirschel, W Kordulla** : *Shear flow in surface-oriented coordinates.* Notes on numerical fluid mechanics, Vol 4, Vieweg, 1981.

[17] **D. A. Humphreys, J. P. F. Lindhout** : *Calculation methods for 3D turbulent boundary layers.* Prog. Aerospace Sci. 25, 107-129 (1988)

[18] **V. Iyer, J. Harris** : *Three-dimensional compressible boundary layer calculations to fourth order accuracy on wings and fuselages.* 27th Aerospace Sciences Meeting, January 9-12, 1989/Reno, Nevada AIAA 89-0130

[19] **M. Jelliti** : *Transition du régime laminaire au régime turbulent : effets de la tridimensionnalité et de la compressibilité.* Thèse de l'ENSAE (1986)

[20] **L. J. Johnston** : *An upwind scheme for the three-dimensional boundary layer equations.* International Journal for Numerical Methods in Fluids, Vol 11, 1043-1073 (1990)

[21] **E. Krause** : *Numerical treatment of boundary layer problems.* AGARD Lectures Series 64 in Advances in Numerical Fluid Dynamics (1973)

[22] **H. P. Kreplin, H. Vollmers, H. U. Meier** : *Experimental determination of wall shear stress vectors on an inclined prolate spheroid.* Proc. 5th US/FRG DEA meeting AFFDL-TR-80-3088, (1980), p. 315-332. Numerical Fluid Dynamics (1973)

[23] **R. Legendre** : *Lignes de courant d'un écoulement permanent. Décollement et séparation.* La Rech. Aéro. Nov.-déc. 1977

[24] **J. P. F. Lindhout, E. Boer** : *A program for the computation of a compressible turbulent boundary layer under infinite swept wing conditions.* NLR TR 75090 U (1975)

[25] **J. P. F. Lindhout, G. Moek** : *A method for the calculation of 3D boundary layers on practical wing configurations.* NLR MP 79003 U (1979)

[26] **L. M. Mack** : *Transition prediction and linear stability theory.* AGARD Conference Proceedings 224, NATO, PARIS (1977)

[27] **K. Matsuno** : *A vector-oriented finite difference scheme for calculating three-dimensional compressible laminar and turbulent boundary layers on practical wing configurations.* AIAA paper 81-1020

[28] **H. U. Meier, H. P. Kreplin** : *Experimental investigation of the boundary layer transition and separation on a body of revolution.* 2^{nd} Symposium on Turbulent Shear Flows. London Jul. 1979

[29] **H. U. Meier, H. P. Kreplin, H. Vollmers** : *Development of boundary layer and separation patterns on a body of revolution at incidence.* 2^{nd} Symposium on Numerical and Physical Aspects of Aerodynamic Flows, Long Beach, Jan. 1983

[30] **H. U. Meier, H. P. Kreplin, A. Landhausser, D. Baumgarten** : *Boundary layers developing on a 1:6 prolate spheroide with natural transition.* Rapport interne DFVLR I8 222-84 A10 1984

[31] **V. C. Patel, J. H. Baek** : *Calculation of three-dimensional boundary layers on bodies at incidence.* Iowa Inst. of Hydraulic Research Rept. No 256 (1982)

[32] **D. J. Peake, M. Tobak** : *Three-dimensional interactions and vortical flows with emphasis on high speed.* NASA TM-81169 AGARDograph 252, July 1980.

[33] **P. D. Smith** : *The numerical computation of three-dimensional turbulent boundary layers.* In: IUTAM Symposium on Three Dimensional Turbulent Boundary Layers. Springer Verlag, 1982, 265-185

[34] **A. Tassa, E. H. Atta, L.A. Lemmerman** : *A new three-dimensional boundary layer calculation method.* AIAA Paper 82-0224

[35] **K. C. Wang** : *On the determination of the zones of influence and dependence for three-dimensional boundary layer equations.* J. Fluid Mech., Vol.48, Part 2, pp. 397-404

[36] **K. C. Wang** : *Boundary layer over a blunt body at low incidence with circumferencial reverse flow.* J. Fluid Mech., Vol.72, Part 1, pp. 49-65